


PARK7 enhances antioxidative-stress processes of BMSCs via the ERK1/2 pathway

Fei Zhang^{1,2} | Wuxun Peng^{1,2}  | Jian Zhang^{1,2} | Lei Wang³ | Wentao Dong^{1,2} | Yinggang Zheng⁴ | Zhenwen Wang⁵ | Zhihong Xie² | Tao Wang² | Chuan Wang² | Yanglin Yan²

¹Department of Traumatologic Surgery, The Affiliated Hospital of Guizhou Medical University, Guiyang, Guizhou, China

²School of clinical medicine, Guizhou Medical University, Guiyang, Guizhou, China

³Department of Statistics, Guizhou Maternal and Child Health Hospital, Guiyang, Guizhou, China

⁴Department of Orthopedics, The Affiliated Wudang Hospital of Guizhou Medical University, Guiyang, Guizhou, China

⁵Department of Orthopedics, The Affiliated Cancer Hospital of Guizhou Medical University, Guiyang, Guizhou, China

Correspondence

Wuxun Peng, Department of Traumatologic Surgery, The Affiliated Hospital of Guizhou Medical University, Guizhou Medical University, Guiyang, 550004 Guizhou, China.
Email: 903463644@qq.com

Funding information

Special Project of Academic New Seedling Cultivation and Innovation Exploration of Guizhou Medical University in 2018, Grant/Award Number: [2018]5779-43; Guiyang Science and Technology Bureau-Guizhou Medical University Joint Fund, Grant/Award Number: [2017]5-2; Science and Technology Fund of Guizhou Provincial Department of Health, Grant/Award Numbers: gzwjkj2018-1-008, gzwjkj2019-1-135; National Natural Science Foundation of China, Grant/Award Numbers: 81860387, 81902226

Abstract

Oxidative stress in the microenvironment surrounding lesions induces apoptosis of transplanted bone-marrow-derived mesenchymal stem cells (BMSCs). Hence, there is an urgent need for improving antioxidative-stress processes of transplanted BMSCs to further promote their survival. The present study reports the role and mechanism of Parkinson's disease protein 7 (PARK7) in enhancing antioxidative activity in BMSCs. We used a PARK7 lentivirus to transfect BMSCs to up- or downregulate PARK7, and then used H₂O₂ to simulate oxidative stress in BMSCs in vitro. Overexpression of PARK7 effectively reduced reactive oxygen species and malondialdehyde, protected mitochondrial membrane potential, and resisted oxidative-stress-induced apoptosis of BMSCs, but the expression of PARK7 was downregulated, these results were reversed. At the same time, we also found that overexpression of PARK7 increased extracellular-regulated protein kinase 1/2 (ERK1/2) phosphorylation and nuclear translocation, as well as upregulated Elk1 phosphorylation and superoxide dismutase (SOD) expression. In contrast, when U0126 was used to block the ERK1/2 pathway, ERK1/2 and Elk1 phosphorylation levels were downregulated, ERK1/2 nuclear translocation and SOD content were significantly reduced, and PARK7-overexpression-induced antioxidative activity was completely blocked. Collectively, our results suggest that PARK7 overexpression increased antioxidative-stress processes and survival of BMSCs subjected to H₂O₂ via activating the ERK1/2 signaling pathway. Our findings may guide the development of a PARK7-specific strategy for improving the transplantation efficacy of BMSCs.

KEYWORDS

bone-marrow-derived mesenchymal stem cells, extracellular-regulated protein kinase 1/2, oxidative stress, Parkinson's disease protein 7

This is an open access article under the terms of the Creative Commons Attribution-NonCommercial-NoDerivs License, which permits use and distribution in any medium, provided the original work is properly cited, the use is non-commercial and no modifications or adaptations are made.

© 2020 The Authors. *Journal of Cellular Biochemistry* Published by Wiley Periodicals LLC

1 | INTRODUCTION

Bone-marrow-derived mesenchymal stem cells (BMSCs) have a strong regenerative ability and exhibit promising therapeutic potential for repairing damaged tissues.^{1–4} However, an oxidative-stress microenvironment exists at lesion sites and greatly limits the survival and efficacy of transplanted BMSCs.^{5–9} Hence, there is an urgent need for improving antioxidative-stress processes of transplanted BMSCs to further promote their survival and efficacy.

At present, approaches for ameliorating oxidative stress have mainly consisted of pretreatments of antioxidants and other drugs that primarily inhibit apoptotic pathways; however, the efficacies of such treatments have been unsatisfactory due to them not being sustainable over time.^{10,11} Parkinson's disease protein 7 (PARK7) is a homodimer comprised of 189 amino acids, is highly conserved, and is widely expressed in various cells and tissues, including BMSCs. Functionally, PARK7 is an extensive oxygen scavenger, antioxidative-stress protein, and plays an important role in cellular survival.^{12,13} Studies in neurons and cardiomyocytes have shown that overexpression of PARK7 significantly reduces the levels of reactive oxygen species (ROS) and malondialdehyde (MDA), increases the expression of superoxide dismutase (SOD) and catalase (CAT), improves the antioxidative-stress processes of cells, and promotes survival of cells under oxidative stress; in contrast, PARK7 deficiency leads to reduced antioxidative-stress activity, premature senescence, and apoptosis of cells under oxidative stress.^{14–16} However, the effects and mechanisms of PARK7 on antioxidative-stress processes in BMSCs are currently unknown.

In the present study, BMSCs were cultured and treated with H₂O₂ to simulate oxidative stress *in vitro*. The effects and mechanisms of PARK7 on antioxidative-stress processes in BMSCs were investigated via gene-overexpression and short-hairpin RNA (shRNA) techniques. Our findings demonstrate that upregulating PARK7 may represent a promising strategy for improving the transplantation efficacy of BMSCs.

2 | METHODS

2.1 | Animals

Male Sprague–Dawley (SD) rats (2-week old) were provided by the Laboratory Animal Center of Guizhou Medical University. The experiment approved by the Experimental Animal Ethics Committee of Guizhou Medical University (No. 1900677), and the experimental

facility certificate number is SYXK (Qian) 2018-0001. All procedures were performed in accordance with our Institutional Guidelines for Animal Research, and the investigation conformed to the Guide for the Care and Use of Laboratory Animals published by the US National Institutes of Health (NIH Publication No. 85-23, revised in 1996).

2.2 | Reagents and instruments

Low glucose Dulbecco's modified Eagle's medium (L-DMEM; Gibco), fetal bovine serum (FBS; Gibco), trypsin (Gibco), double antibody (Hyclon), phosphate-buffered saline (PBS; Hyclon), percoll separation solution (Pharmacia), heparin (Solarbio), dimethyl sulfoxide (Sigma), cell counting kit-8 (CCK-8) solution (Solarbio), 30% hydrogen peroxide solution (Chengdu Jinshan Chemical Reagent Co., Ltd.), terminal deoxynucleotidyl transferase biotin-dUTP nick end labeling (TUNEL; Beytime), 4',6'-diamidino-2-phenylindole (DAPI; Solarbio). Reactive oxygen species detection kit (Sigma), cell apoptosis mitochondrial membrane potential detection kit (KeyGen BioTech), MDA test kit (Beytime), osteogenic differentiation medium of SD rat bone marrow mesenchymal stem cells (Cyagen Biosciences), adipogenic differentiation medium of SD rat bone marrow mesenchymal stem cells (Cyagen Biosciences), chondrogenic differentiation medium of SD rat bone marrow mesenchymal stem cells (Cyagen Biosciences), BCA protein quantification kit (Solarbio). Rabbit PARK7 primers (Sangon Biotech), M-MuLV RT master mix (Sangon Biotech), SYBR green mix (Sangon Biotech). Hamster anti-rat CD29-AF647 (BD), mouse anti-rat CD90-PECyTM7 (BD), mouse anti-rat CD106-PE (BD), mouse anti-rat CD11b-V450 (BD), mouse anti-rat CD45-FITC (BD), mouse anti-rat PARK7 (Abcam), mouse anti-rat SOD2 (Abcam), mouse anti-rat MEK1/2 (Cell Signaling Technology), rabbit anti-rat p-MEK1/2^{S217/221} (Cell Signaling Technology), rabbit anti-rat p-ERK1/2^{T202/Y204} (Cell Signaling Technology), rabbit anti-rat extracellular-regulated protein kinase 1/2 (ERK1/2; Cell Signaling Technology), rabbit anti-rat Elk1 (Abcam), rabbit anti-rat p-Elk1^{S383} (Abcam), rabbit anti-rat Histone H3 (Abcam), rabbit anti-rat GAPDH (Abcam), mouse anti-rat β -actin (Abcam), sodium dodecyl sulfate polyacrylamide gel electrophoresis (SDS–PAGE; Solarbio), polyvinylidene fluoride (PVDF; Millipore), enhanced chemiluminescence (ECL)(Millipore), Lv-PARK7-EGFP (Shanghai Genechem Co.), Lv-ShPARK7-EGFP (Shanghai Genechem Co.), Eni.s and Polybrane (Shanghai Genechem Co.), puromycin (Shanghai Genechem Co, Ltd). Micro-adjustable pipette (Eppendorf), biosafety cabinet (ESCO), benchtop high-speed

refrigerated centrifuge (Beckman), nucleic acid and protein measuring instrument (Nanodrop), quantitative polymerase chain reaction (qPCR) instrument (Bio-Rad), multi-function microplate reader (Biotech), inverted fluorescence microscope (Zeiss), laser confocal microscope (Zeiss), flow cytometry (Beckman), and gel imaging system (Clinx Science Instruments, Ltd.).

2.3 | Isolation and culture of BMSCs

The male SD rats (2-week old) were anesthetized by intraperitoneal injection of chloral hydrate (10%, 0.5 ml/100 g). Then, the bilateral femurs and tibias were quickly removed under sterile conditions, and the bone marrow cavity was washed with PBS solution containing heparin (1000 U/ml) to obtain bone marrow. The bone marrow was then centrifuged to remove upper suspended fat, which precipitated along the wall of a tube containing Percoll separation solution (1.073 g/ml), which was then centrifuged at 900g/min for 30 min. The nucleated cells were then washed with PBS, after which they were inoculated in complete DMEM (10% fetal bovine serum [FBS] and 1% double antibody). Cells were then cultured at 37°C and 5% CO₂. When the cultured primary BMSCs reached a 80%–90% confluency, the cells were digested at 37°C with an appropriate amount of 0.25% trypsin and 0.02% ethylenediaminetetraacetic acid. The third passage of cultured BMSCs were used for subsequent experiments.

2.4 | Osteogenic differentiation of BMSCs

Third-generation BMSCs were inoculated into six-well plates. When the cellular confluence reached 60%–70%, according to the BMSC osteogenic induction kit, the experimental group was incubated in BMSC osteogenic-differentiation medium, while the control group remained in complete DMEM. After 2 weeks of osteogenic induction, cells were fixed, calcium nodules were identified by 0.1% Alizarin-red staining, and alkaline phosphatase (ALP) activity was detected by a modified Gomori calcium-cobalt method.

2.5 | Adipogenic differentiation of BMSCs

Third-generation BMSCs were inoculated into six-well plates. When the degree of cellular fusion reached 100%,

according to the BMSC adipogenic induction kit, the experimental group was incubated in BMSC adipogenic-differentiation medium, while the control group remained in complete DMEM. After 3 weeks of induction, oil-red-O staining was used to detect intracellular lipid droplets.

2.6 | Chondrogenic differentiation of BMSCs

Third-generation BMSCs were inoculated into six-well plates. When the degree of cellular fusion reached 60%–70%, according to the BMSC chondrogenic induction kit, the experimental group was incubated in BMSC chondrogenic-differentiation medium, while the control group remained in complete DMEM. After 4 weeks of induction, acid mucopolysaccharide in cartilage was detected by Alixin-blue staining.

2.7 | Identification of BMSC surface antigens

Third-generation BMSCs were adjusted to a density of 2×10^7 cells/ml. The control group was incubated in 50 μ l of buffer. The single-label group was incubated in 5 μ l of antibody (hamster anti-rat CD29-AF647, mouse anti-rat CD90-PECy7, mouse anti-rat CD106-PE, mouse anti-rat CD11b-V450, or mouse anti-rat CD45-FITC). Then, 45 μ l of buffer was added separately to each tube. For the mixed label group, 5 μ l of each antibody was added to a single flow tube, after which 25 μ l of buffer was added. Then, 50 μ l of cell suspension was added to each flow tube, incubated in the dark for 30 min at room temperature, washed twice with standing buffer, and then 500 μ l of buffer was added to each tube for detection of surface antigens.

2.8 | Construction of in vitro model of oxidative stress

Third-generation BMSCs were divided into the following four groups once they had reached 80% confluency: control group (0 μ M H₂O₂) and three H₂O₂ groups (500, 1000, and 1500 μ M). BMSCs were treated with DMEM containing different concentrations of H₂O₂ for 24 h. The concentration of H₂O₂ that reduced cellular viability by approximately 50% and increased apoptosis by more than 20% was considered to be the optimal concentration for emulating oxidative stress in vitro.

2.9 | Detection of ROS

BMSCs were washed three times with PBS, stained according to the DCFH-DA fluorescent probe kit, incubated for 30 min (5% CO₂; 37°C), and green fluorescence was observed under a fluorescein isothiocyanate channel using a confocal microscope.

2.10 | CCK-8 assay

BMSCs were washed three times with PBS, and the complete DMEM was replaced. Then, 10 µl of CCK-8 solution was added to each well. After incubation for 3 h, the absorbance value (OD) at 450 nm within each well was measured via a microplate reader.

2.11 | Detection of apoptosis via TUNEL/DAPI

BMSCs were fixed with 4% paraformaldehyde for 30 min at room temperature. Then, 0.3% Triton X-100 was permeated for 6 min. An appropriate amount of TUNNEL detection solution was added, and the reaction was incubated at 37°C for 60 min in the dark. Subsequently, DAPI was added for 4 min. After each step, the cells were washed with PBS. At the end of the procedure, samples were sealed with an anti-fluorescent quenching agent. Fluorescence (red and blue fluorescent channels) was detected under a laser-scanning confocal microscope.

2.12 | Lentiviral transfection of BMSCs

Lv-EGFP, Lv-PARK7-EGFP, and Lv-ShPARK7-EGFP lentiviruses (LVs) were purchased from China Shanghai Genechem Co., Ltd. According to the best MOI (MOI = 80) and the best transfection conditions (Eni.s + polybrane) found in transfection pilot experiments, BMSCs were infected with LVs (and an empty vector was used for the control group). At 12 h after transfections, the culture medium was replaced with complete DMEM. On the fourth day after transfections, stable transfections were screened by adding complete DMEM containing 1.8 µg/ml of puromycin. As the cells in the blank control all died, the concentration of puromycin was reduced to 0.9 µg/ml for continued screening of the stable transfection cells.

2.13 | Quantitative polymerase chain reaction

Extraction of total RNA from BMSCs was performed using column-affinity purification. Complementary DNAs were synthesized using the M-MuLV RT master mix with Oligo(dT). Next, qPCR was performed on a StepOnePlus system in 96-well plates with specific primers and SYBR green mix. The primers were as follows: PARK7-F, AGGCGAGCTGGGATTAAGGT; PARK7-R, GACGACCACATCAT ACGGGC; ACTB-F, TCCCTGGAGAAGAGCTACGA; ACTB-R, GTACAGGTCCTTGC GGATGT. The fold-change value of messenger RNA (mRNA) expression compared to that of the control was calculated following the $\Delta\Delta C_t$ method.

2.14 | Western blot analysis

SDS-PAGE gels were prepared, and an equal amount of protein was added to each lane for electrophoresis and transferred to a PVDF membrane. The following primary antibodies were used: mouse anti-rat PARK7, mouse anti-rat SOD2, mouse anti-rat MEK1/2, rabbit anti-rat p-MEK1/2^{S217/221}, rabbit anti-rat p-ERK1/2^{T202/Y204}, rabbit anti-rat ERK1/2, rabbit anti-rat Elk1, rabbit anti-rat p-Elk1^{S383}, rabbit anti-rat Histone H3, rabbit anti-rat GAPDH, and mouse anti-rat β -actin. Horseradish peroxidase-conjugated rabbit anti-mouse or murine anti-rabbit immunoglobulin G was used for secondary-antibody reactions. An enhanced chemiluminescence (ECL) kit was used for exposure. Finally, images were obtained using a gel-imaging system and were quantified using ImageJ software (1.4.3.67).

2.15 | Detection of MDA

BMSCs were lysed via ultrasound to obtain cellular lysates, as follows: 300-W power was used; the procedure was performed with lysates in an ice-water bath; and the ultrasound lasted for 5 s each time at 30-s intervals, which was repeated four times. Then, 100 µl of lysate was added to an MDA-kit working solution according to the instructions of the MDA test kit, after which the mixture was heated to 100°C for 15 min, cooled in a water bath, centrifuged at 1000 rpm/min for 10 min, and 200 µl of each supernatant was then added to a well in a 96-well plate. The absorbance value at 523 nm was measured via a microplate reader.

2.16 | JC-1 staining for assaying the mitochondrial membrane potential

After the BMSCs were washed with PBS, a JC-1 reaction mixture was prepared according to the instructions of the mitochondrial-membrane-potential detection kit. The reaction mixture was added and incubated at 37°C for 30 min. The cells were subsequently washed three times with PBS, and the fluorescence was observed under a laser-scanning confocal microscope.

2.17 | Statistical analysis

All statistical data were calculated and plotted using GraphPad Prism 6. To assess statistical significance, the Kolmogorov–Smirnov test was used to determine if data sets were normally distributed. Analysis of variance and the appropriate post hoc test were used for analyses that involved comparisons among more than two groups. All data are presented as the mean \pm SD, and $p < .05$ was considered statistically significant.

3 | RESULTS

3.1 | Culturing and identification of BMSCs

According to the international identification criteria of mesenchymal stem cells, we determined the morphologies, surface markers, and multi-differentiation potentials of our third-generation cultured cells. In the present study, BMSCs were isolated and cultured by density-gradient centrifugation combined with adherence methods. The cells exhibited long spindle-shaped and fish-shaped morphologies that were in accordance with those of BMSCs (Figure 1A,B). The surface antigens CD90, CD106, CD45, and CD11b were identified via flow cytometry. Among the analyzed cells, 100% were positive for CD90 and CD106, while $7.27\% \pm 2.06\%$ and $8.68\% \pm 2.58\%$ were positive for CD45 and CD11b, respectively (Figure 1D). Hence, these findings confirmed that our cultured cells expressed typical BMSC surface markers with high purity. Additionally, we identified the multi-differentiation potential of our cultured cells. Osteogenic-induced cells showed orange-red calcium

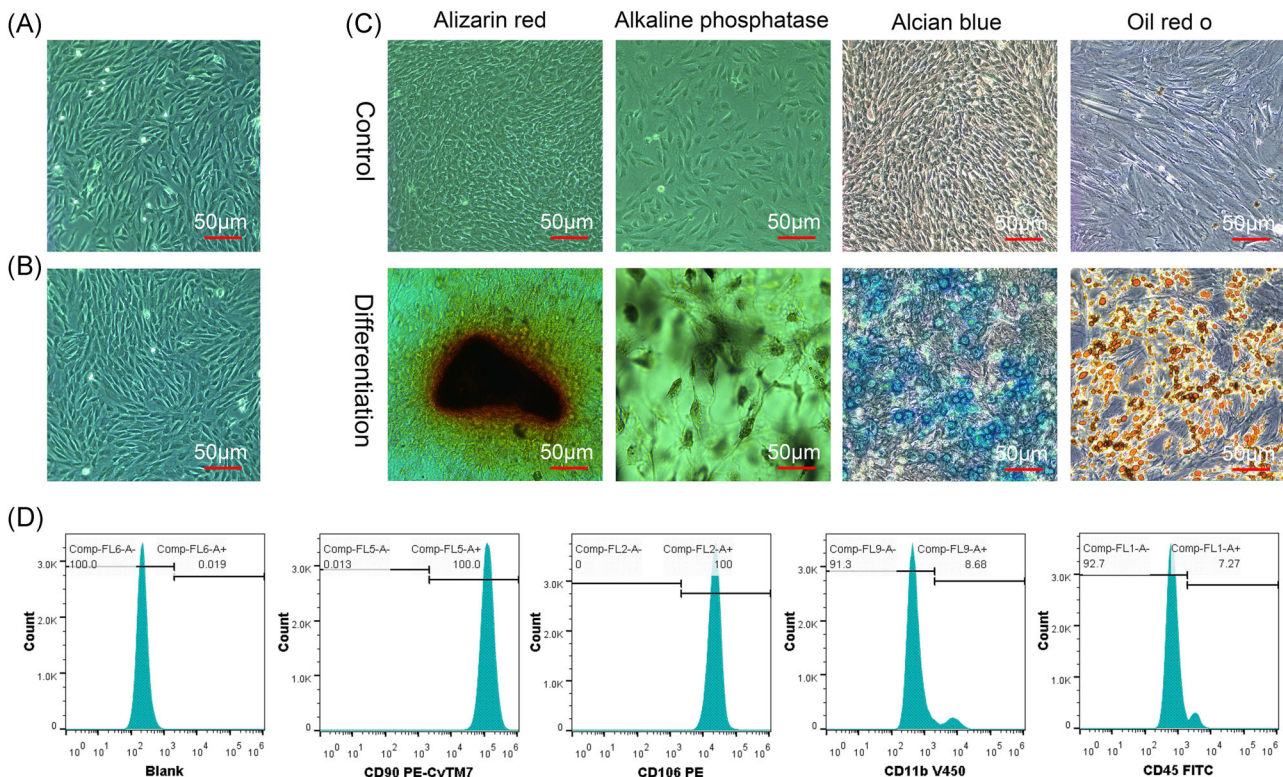


FIGURE 1 Culturing and identification of BMSCs. A, Primary BMSCs are shown. B, Third-generation BMSCs are shown. C, BMSCs were identified by osteogenic, adipogenic, and chondrogenic inductions. D, Flow cytometry identified the following BMSC surface antigens: CD90, CD106, CD45, and CD11b. BMSC, bone-marrow-derived mesenchymal stem cell

nodules after Alizarin-red staining, and black-heterodye particles appeared in the cytoplasm after ALP staining (Figure 1C). Lipogenic-induced cells exhibited different sizes of orange droplets in the cytoplasm after Oil-red-O staining (Figure 1C). Cartilage-induced cells exhibited blue staining of mucopolysaccharides after Alexin-blue staining (Figure 1C). These findings demonstrate that our cultured cells exhibited a multi-differentiation potential that is consistent with that of BMSCs. Based on the above results, we successfully cultured BMSCs with high purity, which we then used for all subsequent experiments.

3.2 | Model of oxidative stress in BMSCs

To explore the optimal concentration of H₂O₂ in emulating oxidative stress in vitro, we incubated third-generation BMSCs in different concentrations of H₂O₂ (0, 500, 1000, and 1500 μM) for 24 h, and then assayed ROS, MDA, cellular viability, and apoptosis. Increasing H₂O₂ concentrations decreased cellular viability (Figure 2E) while increasing ROS (Figures 2A and 2C), MDA (Figure 2F), and apoptosis (Figures 2B and 2D). When the concentration of H₂O₂ was 500 μM, ROS content was increased, cellular viability was higher than 60%, and the apoptotic rate was lower than 20% (Figure 2A–E). When the concentration of H₂O₂ was 1500 μM, ROS content was significantly increased, cellular viability was lower than 15%, and the apoptotic rate was higher than 90% (Figure 2A–E); as such, subsequent experiments could not be carried out at this H₂O₂ concentration. When the concentration of H₂O₂ was 1000 μM, ROS content was increased, cellular viability was 48.41% ± 8.15%, and the apoptotic rate was 36.39% ± 1.16%, compared with the control group, these differences were statistically significant ($p < .05$), which we interpreted to represent our best model for assaying oxidative stress in vitro (Figure 2). Therefore, we employed 1000 μM as our optimal H₂O₂ concentration in all subsequent experiments for assaying Park7-induced changes of oxidative stress in vitro.

3.3 | PARK7 enhances antioxidative-stress processes in BMSCs

We used LV to construct PARK7 overexpression and interference (ie, shRNA) vectors (LV-PARK7 and LV-ShPARK7) and then transfected BMSCs with these LVs. The results showed that there was no significant difference in PARK7 mRNA and protein levels between

LV-EGFP group and the control group, while PARK7 mRNA and protein levels in the LV-PARK7 group were upregulated by approximately 10-fold ($p < .05$) and 2-fold ($p < .05$), respectively. In the LV-ShPARK7 group, PARK7 mRNA and protein levels were downregulated by 81.3% ($p < .05$) and 62.5% ($p < .05$; Figure 3A–C), respectively. Subsequently, we used H₂O₂ (1000 μM) incubations for 24 h to simulate an oxidative-stress microenvironment in BMSCs. The results showed that the mitochondrial membrane potential of LV-PARK7 group was higher than that of control group (Figure 3D,E), whereas intracellular ROS and MDA levels were reduced (Figures 4A, 4B, and 4F), cellular viability was increased (Figure 4C), and apoptosis rates were decreased (12.12% ± 6.44%; $p < .05$ for all parameters; Figures 4D,E). In contrast none of these parameters were significantly changed in the Lv-EGFP group. Next, compared to those of the control group, shRNA knockdown of PARK7 increased ROS and MDA levels, decreased both cellular viability and mitochondrial membrane potential, and increased apoptosis rates by 88.75% ± 5.47% ($p < .05$ for all parameters; Figures 3 and 4). These results indicate that PARK7 enhanced the antioxidative stress ability of BMSCs and promote the survival of BMSCs under oxidative stress conditions.

3.4 | PARK7 activates ERK1/2 signaling pathway to enhance antioxidative stress processes of BMSCs

To further investigate whether PARK7 enhanced antioxidative-stress processes in BMSCs through the ERK1/2 pathway, we treated LV-PARK7-overexpression BMSCs with H₂O₂ (1000 μM) and then assayed the phosphorylation levels of MEK1/2, ERK1/2, and ELK1—as well as the nuclear translocation of ERK1/2 and SOD—via western blot analysis. Compared with those of the control group, the phosphorylation levels of MEK1/2, ERK1/2, and ELK1 in the Lv-PARK7-overexpression group were upregulated (Figure 5A); additionally, ERK1/2 nuclear translocation (Figures 5B, 5C, and 5E) and SOD content were both increased (Figures 5A and 5D). When we treated the Lv-PARK7-overexpression group with a MEK1/2 inhibitor (U0126), SOD content and the phosphorylation levels of MEK1/2, ERK1/2, and ELK1 were significantly reduced (Figure 5), indicating that inhibition of the ERK1/2 pathway blocked the protective effect of PARK7 overexpression on oxidative-stress damage in BMSCs. In conclusion, these findings suggest that PARK7 may enhance antioxidant-stress processes and cellular survival of BMSCs under

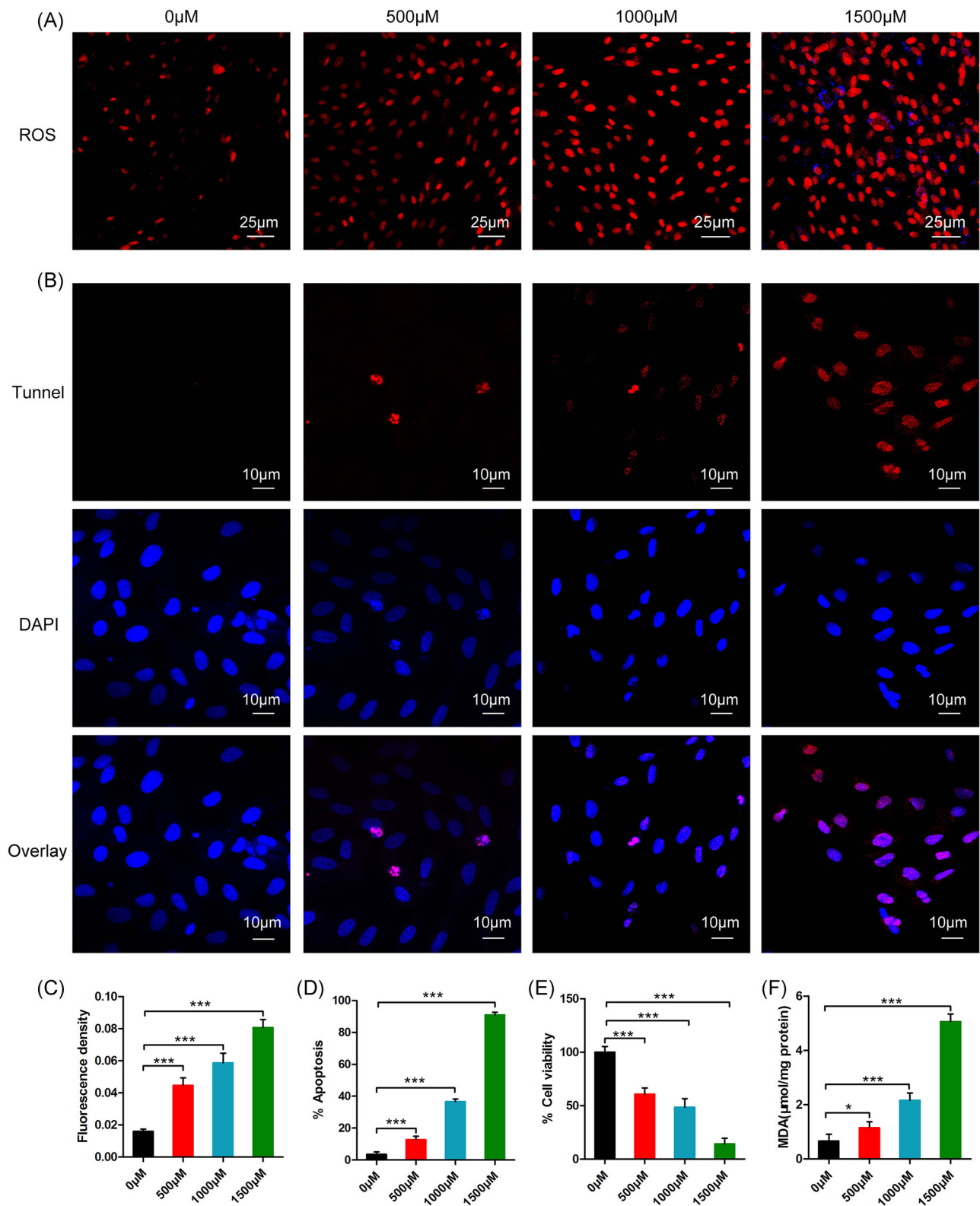


FIGURE 2 Model of oxidative in BMSCs. A, DHE was used to detect intracellular ROS ($n = 4$). B, Terminal deoxynucleotidyl transferase dUTP nick-end labeling (Tunnel)/DAPI was used to detect apoptosis ($n = 4$). C, A histogram of ROS is shown ($n = 4$). D, A histogram of apoptosis is shown ($n = 4$). E, A CCK-8 assay was used to measure cellular viability ($n = 5$). (F) Detection of MDA content is shown ($n = 5$). In (C–F), data are presented as the mean \pm SD. Statistical significance was determined via ANOVA. Data from experimental groups were compared with those of the control group (0 μ M). ANOVA, analysis of variance; CCK-8, cell counting kit-8; DAPI, 4',6-diamidino-2-phenylindole; DHE, dihydroethidium; MDA, malondialdehyde; ROS, reactive oxygen species; TUNEL, terminal deoxynucleotidyl transferase dUTP nick-end labeling. * $p < .05$, *** $p < .001$

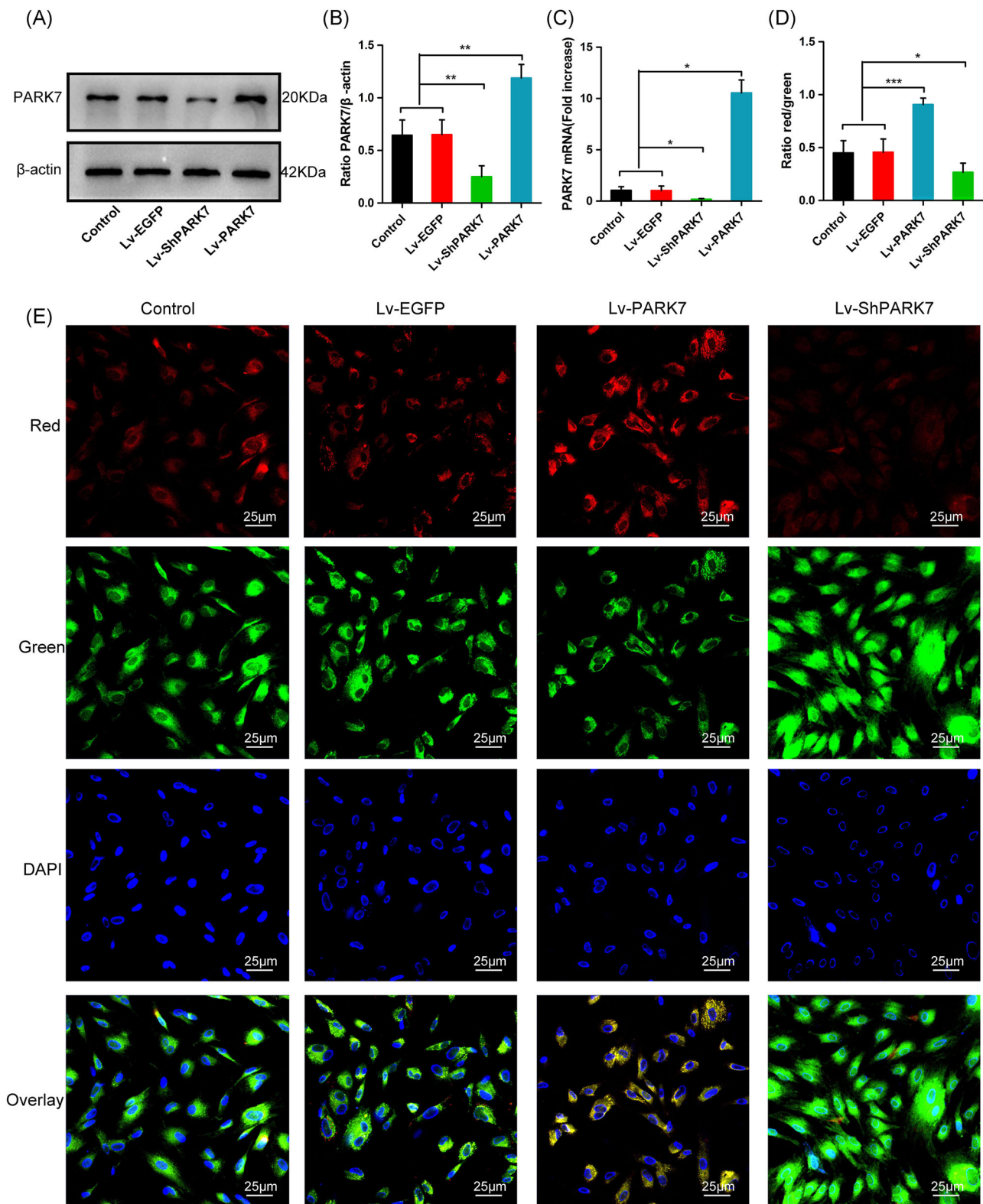


FIGURE 3 Effect of PARK7 on the mitochondrial membrane potential. A, Western blot analysis was used to detect the protein expression of PARK7 ($n = 3$). B, Analysis of PARK7 protein expression is shown ($n = 3$). C, qPCR was used to detect PARK7 mRNA levels ($n = 3$). (D–E) JC-1 staining was used to assay the mitochondrial membrane potential of BMSCs ($n = 4$). In (B–D), data are presented as the mean \pm SD. Statistical significance was determined via ANOVA. Data from experimental groups were compared with those of the control group (nontransfected BMSCs) and Lv-EGFP groups. ANOVA, analysis of variance; BMSC, bone-marrow-derived mesenchymal stem cell; mRNA, messengerRNA; PARK7, Parkinson's disease protein 7; qPCR, quantitative polymerase chain reaction. * $p < .05$, ** $p < .01$, *** $p < .001$

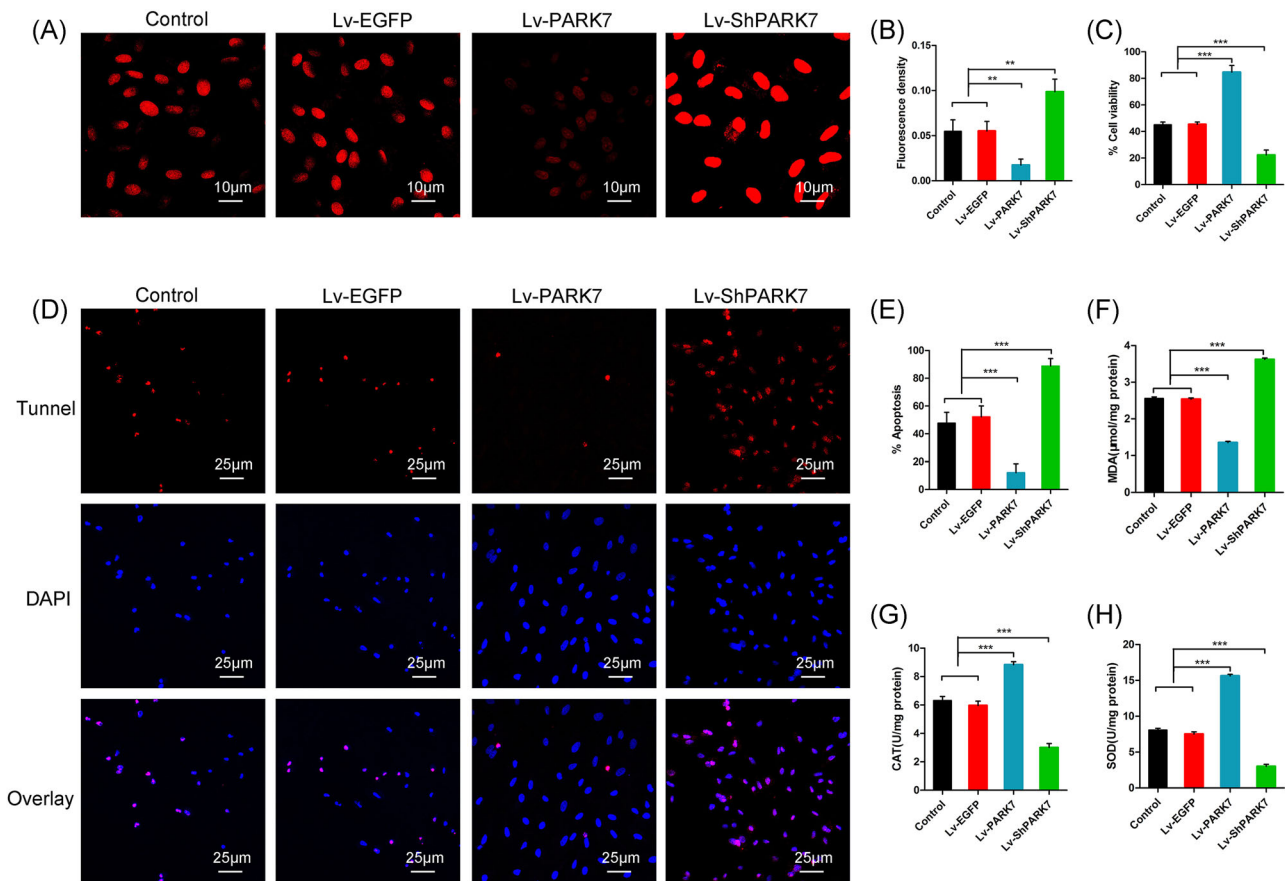


FIGURE 4 Effect of PARK7 on antioxidative-stress processes of BMSCs. A, DHE was used to detect intracellular ROS ($n = 4$). B, Analysis of ROS fluorescent intensities ($n = 4$) is shown. C, A CCK-8 assay was used to measure cellular viability ($n = 4$). D, TUNEL/DAPI was used to detect apoptosis ($n = 4$). E, Analysis of apoptotic rates ($n = 4$) is shown. F, Detection of MDA content ($n = 4$) is shown. G, CAT activity analysis ($n = 4$) is shown. H, SOD activity analysis ($n = 4$) is shown. In (B), (C), and (E–H), data are presented as the mean \pm SD. Statistical significance was determined via analysis of ANOVA. Data from experimental groups were compared with those of the control group (non-transfected BMSCs) and Lv-EGFP groups. ANOVA, analysis of variance; BMSC, bone-marrow-derived mesenchymal stem cell; CAT, catalase; CCK-8, cell counting kit-8; DAPI, 4',6-diamidino-2-phenylindole; DHE, dihydroethidium; MDA, malondialdehyde; PARK7, Parkinson's disease protein 7; ROS, reactive oxygen species; SOD, superoxide dismutase; TUNEL, terminal deoxynucleotidyl transferase dUTP nick-end labeling. ** $p < .01$, *** $p < .001$

oxidative stress via activating the ERK1/2 signaling pathway.

4 | DISCUSSION

Clinically, BMSCs have been used in the treatment of various diseases. However, the oxidative-stress micro-environment surrounding lesions induces apoptosis of transplanted BMSCs, which severely limits the efficacy of BMSC transplantations.^{17,18} Hence, improving antioxidative-stress processes of transplanted BMSCs is key to improving their efficacies following transplantation.^{19–21} In the present study, PARK7 was upregulated or downregulated via lentiviral transfections in BMSCs, after which BMSCs were treated with H₂O₂ to simulate

oxidative stress in vitro. Our results suggested that PARK7 overexpression enhanced antioxidative-stress processes in BMSCs via activation of the ERK1/2 signal pathway, effectively reduced ROS and MDA, protected the mitochondrial membrane potential, and ameliorated apoptosis of BMSCs subjected to H₂O₂.

A central hallmark of oxidative stress is the production of excessive ROS.^{22–24} Excessive ROS can change the redox state in cells, which damages DNA, proteins, lipids, and other biological macromolecules. ROS-induced damage of mitochondria can lead to dysfunction of the mitochondrial electron-transport chain, decreased transmembrane potential, and aberrant membrane permeability. These ROS-induced pathologies can then lead to the release of apoptosis-inducing factors and activation of p53, p38MAPK, and DNA damage

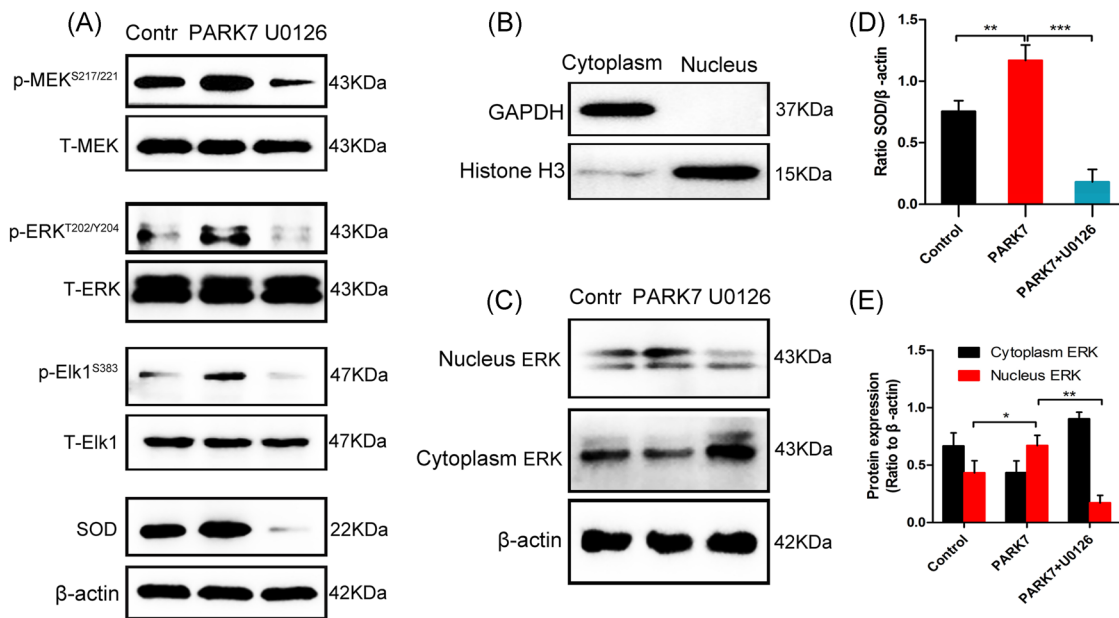


FIGURE 5 PARK7-induced enhancement of antioxidant-stress processes in BMSCs is blocked via inhibition of the ERK1/2 signaling pathway. **A**, The phosphorylation levels of MEK1/2, ERK1/2, and ELK1 and expression levels of SOD were detected by western blot analysis ($n = 3$). **B**, western-blot analysis of cytosolic proteins and nuclear proteins ($n = 3$). **C**, Western blot analysis was used to detect the nuclear translocation of ERK1/2 ($n = 3$). **D**, A histogram of SOD protein expression is shown ($n = 3$). **E**, A histogram of ERK1/2 nuclear translocation is shown ($n = 3$). In **(D)** and **(E)**, data are presented as the mean \pm *SD*. Statistical significance was determined via ANOVA. Data from experimental groups were compared with those of the control group (Lv-EGFP). ANOVA, analysis of variance; BMSC, bone-marrow mesenchymal stem cell; Elk1, ETS domain-containing protein Elk-1; ERK1/2, extracellular signal-regulated kinase 1/2; GAPDH, glyceraldehyde 3-phosphate dehydrogenase; MEK1/2, MAP kinase-ERK kinase; PARK7, Parkinson's disease protein 7; SOD, superoxide dismutase. * $p < .05$, ** $p < .01$, *** $p < .001$

response pathways, leading to cellular stress-induced apoptosis and senescence.^{25–31} At present, methods for enhancing antioxidative-stress processes of BMSCs mainly include pretreatments with antioxidants and other drugs. For example, Kim et al.¹¹ pretreated BMSCs with lycopene, which partially improved antioxidative-stress processes of BMSCs but ultimately did not have a long-lasting protective effect. Additionally, Yang et al.¹³ used phenylbutyrate pretreatments to reduce oxidative-stress damage in brain tissue, which was found to be due to upregulation of PARK7. In the present study, BMSCs were transfected with PARK7 LVs to overexpress PARK7, and then H₂O₂ was used to simulate oxidative stress in vitro. The results showed that PARK7 protein in the Lv-PARK7-overexpression group was upregulated by approximately twofold compared to that of the control group. Overexpression of PARK7 effectively reduced ROS and MDA, protected the mitochondrial membrane potential, and reduced apoptosis of BMSCs under oxidative stress. Moreover, our present study used a lentiviral integrase to integrate the PARK7-overexpression construct into the BMSCs genome, which allows for stable expression of this construct in BMSCs to enable long-term enhancement of antioxidative-stress processes that

previously published pharmacological pretreatments have been unable to sustain.

Studies in neurons, cardiomyocytes and renal tubular epithelial cells have shown that PARK7 can be used as a “sensor” of antioxidant stress through autooxidation to activate ERK1/2, nuclear factor erythroid 2-related factor 2, apoptosis signal-regulating kinase 1, phosphatidylinositol 3-kinases /protein kinase B, and other signaling pathways to improve antioxidative processes within cells, thereby inhibiting apoptosis and promoting cellular survival.^{14,32–34} In the present study, our results showed that overexpression of PARK7 upregulated the phosphorylation levels of MEK1/2, ERK1/2, and ELK1, as well as increased ERK1/2 nuclear translocation and SOD content while decreasing apoptosis. Subsequently, we showed that treating BMSCs with an ERK1/2 pathway inhibitor (U0126) effectively blocked the protective effect of PARK7 overexpression on oxidative-stress injury in BMSCs. Our present findings suggest that PARK7 enhances antioxidative-stress processes of BMSCs via activating the ERK1/2 signaling pathway, thereby promoting survival of BMSCs under oxidative stress (Figure 6).

In conclusion, we collectively found that PARK7 overexpression improved antioxidative-stress processes

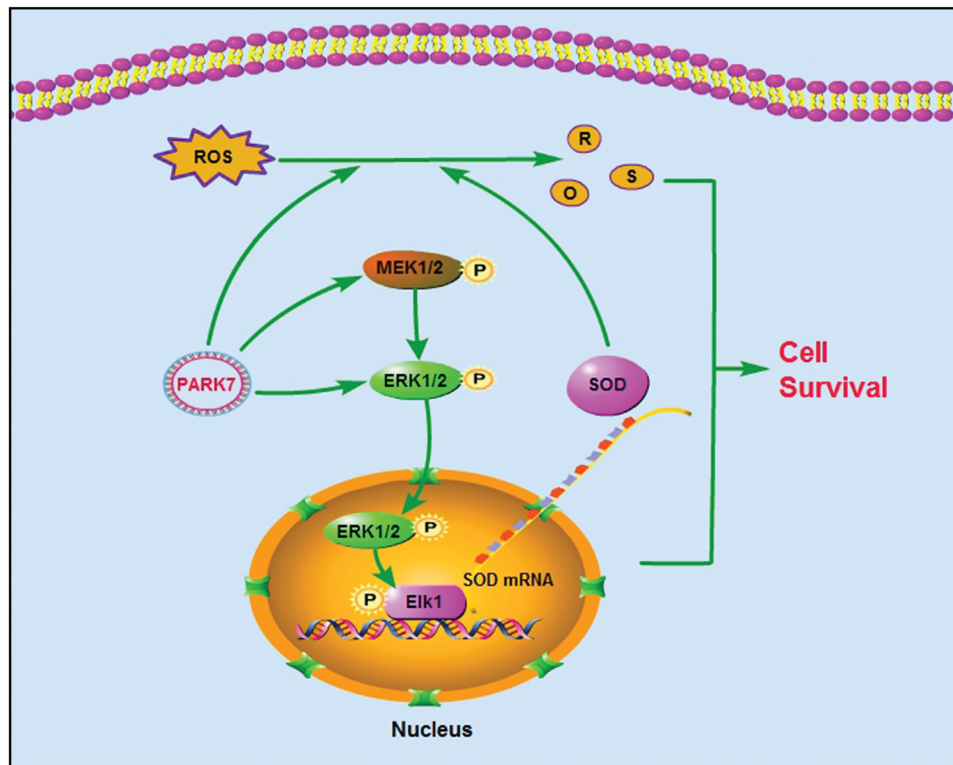


FIGURE 6 Hypothetical model of PARK7 enhancing antioxidative-stress processes in BMSCs. A hallmark of oxidative stress is excessive production of ROS. PARK7 promotes the phosphorylation of MEK1/2 and ERK1/2. Phosphorylated ERK1/2 is then transferred to the nucleus, which phosphorylates the downstream effector, Elk1. Phosphorylated Elk1 then promotes the expression of antioxidative enzymes, such as SOD. Antioxidative proteins, such as PARK7 and SOD, then eliminate excessive intracellular ROS, thereby promoting the survival of BMSCs under oxidative-stress conditions. BMSC, bone marrow-derived mesenchymal stem cell; Elk1, ETS domain-containing protein Elk-1; ERK1/2, extracellular signal-regulated kinase 1/2; MEK1/2, MAP kinase-ERK kinase; PARK7, Parkinson's disease protein 7; ROS, reactive oxygen species; SOD, superoxide dismutase

in BMSCs by the activating of the ERK1/2 signaling pathway, effectively reduced ROS/MDA, protected the mitochondrial membrane potential, and reduced apoptosis of BMSCs subjected to oxidative stress *in vitro*.

ACKNOWLEDGEMENT

This study was supported by the National Natural Science Foundation of China (81902226, 81860387), the Science and Technology Fund of Guizhou Provincial Department of Health (gzwjkj2018-1-008, gzwjkj2019-1-135), the Guiyang Science and Technology Bureau-Guizhou Medical University Joint Fund ([2017]5-2), and the Special Project of Academic New Seedling Cultivation and Innovation Exploration of Guizhou Medical University in 2018 (Qiankehe Platform Talents; [2018]5779-43). This experiment was completed in the Clinical Medicine Research Center of Guizhou Medical University. Thanks to the guidance of the teachers of this center.

CONFLICT OF INTERESTS

The authors declare that there are no conflict of interests.

AUTHOR CONTRIBUTIONS

Fei Zhang and Wuxun Peng designed the experiments. Fei Zhang drafted the manuscript. Wuxun Peng revised the manuscript. Jian Zhang, Lei Wang, and Wentao Donga analyzed the data. Yinggang Zhengd, Zhenwen Wange, Tao Wang, Zhihong Xie, Chuan Wang, and Yanglin Yan performed experiments.

DATA AVAILABILITY STATEMENT

All data generated or analyzed during this study are included in this published article. All data and reagents are available from the corresponding author upon reasonable request.

ETHICS APPROVAL STATEMENT

All experimental procedures for handling and care of mice were done following the instructions of the Institutional Animal Care Committee and approved by the Ethics Committee of the Guizhou Medical University of China (Permission Number: 1800815, valid period: 01,01,2017-12,31,2019).

ORCID

Wuxun Peng  <http://orcid.org/0000-0001-9468-2580>

REFERENCES

- He JG, Li HR, Han JX, et al. GATA-4-expressing mouse bone marrow mesenchymal stem cells improve cardiac function after myocardial infarction via secreted exosomes. *Sci Rep*. 2018;8:9047.
- Hu M, Guo G, Huang Q, et al. The harsh microenvironment in infarcted heart accelerates transplanted bone marrow mesenchymal stem cells injury: the role of injured cardiomyocytes-derived exosomes. *Cell Death Dis*. 2018;9:357.
- Li J, Huang Z, Chen L, Tang X, Fang Y, Liu L. Restoration of bone defects using modified heterogeneous deproteinized bone seeded with bone marrow mesenchymal stem cells. *Am J Transl Res*. 2017;9:3200-3211.
- Peng WX, Wang L. Adenovirus-mediated expression of BMP-2 and BFGF in bone marrow mesenchymal stem cells combined with demineralized bone matrix for repair of femoral head osteonecrosis in beagle dogs. *Cell Physiol Biochem*. 2017;43:1648-1662.
- Hu XF, Wang L, Xiang G, Lei W, Feng YF. Angiogenesis impairment by the NADPH oxidase-triggered oxidative stress at the bone-implant interface: Critical mechanisms and therapeutic targets for implant failure under hyperglycemic conditions in diabetes. *Acta Biomater*. 2018;73:470-487.
- Deng G, Niu K, Zhou F, et al. Treatment of steroid-induced osteonecrosis of the femoral head using porous Se@SiO₂ nanocomposites to suppress reactive oxygen species. *Sci Rep*. 2017;7:43914.
- Li R, Lin QX, Liang XZ, et al. Stem cell therapy for treating osteonecrosis of the femoral head: From clinical applications to related basic research. *Stem Cell Res Ther*. 2018;9:291.
- McGarry T, Biniecka M, Veale DJ, Fearon U. Hypoxia, oxidative stress and inflammation. *Free Radic Biol Med*. 2018;125:15-24.
- Wauquier F, Leotoing L, Coxam V, Guicheux J, Wittrant Y. Oxidative stress in bone remodelling and disease. *Trends Mol Med*. 2009;15:468-477.
- Zhang F, Peng W, Zhang J, et al. New strategy of bone marrow mesenchymal stem cells against oxidative stress injury via Nrf2 pathway: oxidative stress preconditioning. *J Cell Biochem*. 2019;120:19902-19914.
- Kim JY, Lee JS, Han YS, et al. Pretreatment with lycopene attenuates oxidative stress-induced apoptosis in human mesenchymal stem cells. *Biomol Ther*. 2015;23:517-524.
- Jeong HJ, Kim DW, Kim MJ, et al. Protective effects of transduced Tat-DJ-1 protein against oxidative stress and ischemic brain injury. *Exp Mol Med*. 2012;44:586-593.
- Yang RX, Lei J, Wang BD, et al. Pretreatment with sodium phenylbutyrate alleviates cerebral ischemia/reperfusion injury by upregulating DJ-1 protein. *Front Neurol*. 2017;8:256.
- Shen ZY, Sun Q, Xia ZY, et al. Overexpression of DJ-1 reduces oxidative stress and attenuates hypoxia/reoxygenation injury in NRK-52E cells exposed to high glucose. *Int J Mol Med*. 2016;38:729-736.
- Xu X, Martin F, Friedman JS. The familial Parkinson's disease gene DJ-1 (PARK7) is expressed in red cells and plays a role in protection against oxidative damage. *Blood Cells Mol Dis*. 2010;45:227-232.
- Yu HH, Xu Q, Chen HP, et al. Stable overexpression of DJ-1 protects H9c2 cells against oxidative stress under a hypoxia condition. *Cell Biochem Funct*. 2013;31:643-651.
- Liu Y, Zhang X, Chen J, Li T. Inhibition of mircoRNA-34a enhances survival of human bone marrow mesenchymal stromal/stem cells under oxidative stress. *Med Sci Monit*. 2018;24:264-271.
- Shen Y, Jiang X, Meng L, Xia C, Zhang L, Xin Y. Transplantation of bone marrow mesenchymal stem cells prevents radiation-induced artery injury by suppressing oxidative stress and inflammation. *Oxid Med Cell Longev*. 2018;2018:5942916.
- Fan L, Zhang C, Yu Z, Shi Z, Dang X, Wang K. Transplantation of hypoxia preconditioned bone marrow mesenchymal stem cells enhances angiogenesis and osteogenesis in rabbit femoral head osteonecrosis. *Bone*. 2015;81:544-553.
- Wang T, Teng S, Zhang Y, Wang F, Ding H, Guo L. Role of mesenchymal stem cells on differentiation in steroid-induced avascular necrosis of the femoral head. *Exp Ther Med*. 2017;13:669-675.
- Xing M, Wang X, Wang E, Gao L, Chang J. Bone tissue engineering strategy based on the synergistic effects of silicon and strontium ions. *Acta Biomater*. 2018;72:381-395.
- Marrocco I, Altieri F, Peluso I. Measurement and clinical significance of biomarkers of oxidative stress in humans. *Oxid Med Cell Longev*. 2017;2017:6501046.
- Newsholme P, Cruzat VF, Keane KN, Carlessi R, de Bittencourt PI, Jr. Molecular mechanisms of ROS production and oxidative stress in diabetes. *Biochem J*. 2016;473:4527-4550.
- Tönnies E, Trushina E. Oxidative stress, synaptic dysfunction, and Alzheimer's disease. *J Alzheimers Dis*. 2017;57:1105-1121.
- Bu H, Wedel S, Cavinato M, Jansen-Dürr P. microRNA regulation of oxidative stress-induced cellular senescence. *Oxid Med Cell Longev*. 2017;2017:2398696.
- Correia-Melo C, Marques FD, Anderson R, et al. Mitochondria are required for pro-ageing features of the senescent phenotype. *EMBO J*. 2016;35:724-742.
- Korolchuk VI, Miwa S, Carroll B, von Zglinicki T. Mitochondria in cell senescence: is mitophagy the weakest link? *EBioMedicine*. 2017;21:7-13.
- Liguori I, Russo G, Curcio F, et al. Oxidative stress, aging, and diseases. *Clin Interv Aging*. 2018;13:757-772.
- Oh J, Lee YD, Wagers AJ. Stem cell aging: mechanisms, regulators and therapeutic opportunities. *Nat Med*. 2014;20:870-880.
- Sung YJ, Kao TY, Kuo CL, et al. Mitochondrial Lon sequesters and stabilizes p53 in the matrix to restrain apoptosis under oxidative stress via its chaperone activity. *Cell Death Dis*. 2018;9:697.
- Tian Z, Chen Y, Yao N, et al. Role of mitophagy regulation by ROS in hepatic stellate cells during acute liver failure. *Am J Physiol Gastrointest Liver Physiol*. 2018;315:G374-G384.
- Klawitter J, Klawitter J, Agardi E, et al. Association of DJ-1/PDEN/AKT- and ASK1/p38-mediated cell signalling with ischaemic cardiomyopathy. *Cardiovasc Res*. 2013;97:66-76.

33. Oh SE, Park HJ, He L, Skibiel C, Junn E, Mouradian MM. The Parkinson's disease gene product DJ-1 modulates miR-221 to promote neuronal survival against oxidative stress. *Redox Biol.* 2018;19:62-73.
34. Zeng J, Zhao H, Chen B. DJ-1/PARK7 inhibits high glucose-induced oxidative stress to prevent retinal pericyte apoptosis via the PI3K/AKT/mTOR signaling pathway. *Exp Eye Res.* 2019;2019:107830.

How to cite this article: Zhang F, Peng W, Zhang J, et al. PARK7 enhances antioxidative-stress processes of BMSCs via the ERK1/2 pathway. *J Cell Biochem.* 2021;122:222-234. <https://doi.org/10.1002/jcb.29845>